# A generic model of global earthquake rupture characteristics revealed by machine learning

Zefeng Li[1,1]

[1]Univerisity of Science and Technology of China

December 1, 2022

**Abstract**

Rupture processes of global large earthquakes have been observed to exhibit great variability, whereas recent studies suggest that the average rupture behavior could be unexpectedly simple. To what extent do large earthquakes share common rupture characteristics? Here we use a machine learning algorithm to derive a generic model of global earthquake source time functions. The model indicates that simple and homogeneous ruptures are pervasive whereas complex and irregular ruptures are relatively rare. Despite the standard long-tail and near-symmetric moment release processes, the model reveals two special rupture types: runaway earthquakes with weak growing phases and relatively abrupt termination, and complex earthquakes with all faulting mechanisms but mostly shallow origins (<40 km). The diversity of temporal moment release patterns imposes a limit on magnitude predictability in earthquake early warning. Our results present a panoptic view on the collective similarity and diversity in the rupture processes of global large earthquakes.



**A generic model of global earthquake rupture characteristics revealed by machine learning**

**Zefeng Li[1,2*]**

*Laboratory of Seismology and Physics of Earth's Interior, School of Earth and Space Sciences, University of Science and Technology of China, Hefei, China*

*Mengcheng National Geophysical Observatory, University of Science and Technology of China, Mengcheng, China*

*Manuscript submitted to GRL*

*Corresponding author: Zefeng Li (zefengli@ustc.edu.cn)

**Highlights:**

1. A generic model of characteristic source time functions is derived from global earthquake observations using machine learning.
2. The model presents a panoptic view of the similarity and the diversity in the rupture processes of large earthquakes.
3. The diversity of moment release patterns, together with absolute duration variability, imposes a limit on magnitude predictability in early warning.

**Abstract**

Rupture processes of global large earthquakes have been observed to exhibit great variability, whereas recent studies suggest that the average rupture behavior could be unexpectedly simple. To what extent do large earthquakes share common rupture characteristics? Here we use a machine learning algorithm to derive a generic model of global earthquake source time functions. The model indicates that simple and homogeneous ruptures are pervasive whereas complex and irregular ruptures are relatively rare. Despite the standard long-tail and near-symmetric moment release processes, the model reveals two special rupture types: runaway earthquakes with weak growing phases and relatively abrupt termination, and complex earthquakes with all faulting mechanisms but mostly shallow origins (<40 km). The diversity of temporal moment release patterns imposes a limit on magnitude predictability in earthquake early warning. Our results present a panoptic view on the collective similarity and diversity in the rupture processes of global large earthquakes.

**Plain language summary**

Over the past decades, seismologists have observed great variability in the rupture processes of many large earthquakes. However, some recent studies suggest that the average rupture behavior could be unexpectedly simple. Can the average behavior be representative of most earthquakes? To what extent do large earthquakes share common rupture characteristics? Here we use machine learning to derive a panoptic picture, i.e. a generic model of source time functions, for global earthquakes. The model shows that simple and homogeneous ruptures are pervasive whereas complex and irregular ruptures are relatively rare. Besides, it reveals two special rupture types: runaway earthquakes with weak initial phases, and complex earthquakes with all faulting mechanisms but mostly shallow origins (<40 km). Our results present a panoptic view on the collective similarity and diversity in the rupture processes of global large earthquakes, which affects how well we can predict earthquake magnitude in earthquake early warning.

## Introduction

Large earthquakes start, propagate, and terminate in diverse manners owing to complex interplay between rupture dynamics and fault properties. Over the past decades, observations of large earthquake rupture processes have shown various degrees of peculiarity (Ammon, 2005; Ammon *et al.* , 2006; Meng *et al.* , 2012; Ross *et al.* , 2019), suggesting that each large earthquake probably has its own unique characteristics. However, understanding the general physical laws that govern earthquake phenomena requires derivation of the underlying patterns from the seemingly diverse behaviors (Houston and Vidale, 1994; Vallée, 2013; Meier *et al.* , 2017; Denolle, 2019). The average behaviors, often obtained by stacking a large set of seismological data, tend to show relatively simple characteristics, implying common similarity hidden behind the diverse ruptures (Houston and Vidale, 1994; Meier *et al.* , 2017). The distinct emphases on collective rupture peculiarity and similarity raises a critical question: to what extent do large earthquakes share common rupture characteristics? Answering this question calls for a panoptic view of the variability in the rupture processes of global earthquakes.

Earthquake source time functions (STFs) describes the history of seismic moment release during rupture. As an important observation constraining on the source processes, STFs have been routinely extracted from seismograms for large earthquakes. However, because of the high-dimensionality and great variations of amplitude and duration (Tanioka and Ruff, 1997; Duputel *et al.* , 2013; Vallée, 2013), STFs cannot be compared directly. Hence, comparison is often performed on individual STF properties such as duration, peak amplitude, peaks and skewness (Houston, 2001; Persh and Houston, 2004), as well as other derived parameters, such as scaled energy (Denolle, 2019) and relative radiated energy efficiency (Ye *et al.* , 2018). Although these individual properties constrain specific aspects of earthquake ruptures, it remains challenging to examine the variability of overall moment release processes.

Here we employ a machine learning algorithm, called variational autoencoder (VAE), to illuminate the systematic variability of STF shapes among global earthquakes (Figure 1). We train a VAE with normalized STFs of 3675 M>5.5 global earthquakes from 1992 to 2019 (SCARDEC database, Vallée & Douet, 2016). This trained VAE is applied to another independent database of 112 STF of M>7.0 megathrust earthquakes (Ye *et al.* , 2016; referred to as YE2016), to validate its generalization capability. With the VAE, we derive a standard STF model that contains a systematic set of characteristic shapes accompanied by corresponding earthquake population density. The model exhibits a broad range of rupture characteristics for global earthquakes and sheds light on special classes of earthquakes that have not received sufficient attention before. Moreover, the deviation of individual earthquakes from the standard model is measured by the reconstruction misfit.

Hence, large reconstruction misfits naturally detect earthquakes outside the norm, i.e. earthquakes with unusual rupture processes.

**VAE for STFs**

VAE is widely used in signal and image processing to uncover the intrinsic structure of a large data set (Kingma and Welling, 2014). It consists of an encoder to compress the high-dimensional data into a low-dimensional latent representation and a decoder to reconstruct the high-dimensional data from the latent representation (Figure 1). The bottleneck architecture forces the algorithm to learn the key data characteristics and discards the noise in individual samples. After training, the VAE can take input of virtual latent values (a set of parameters in the bottleneck that encode original data) from a random normal distribution to generate synthetic data constrained by real observations, and therefore belongs to generative learning methods. In geophysics, VAE has been recently used to speed up geophysical inversion (Cheng and Jiang, 2020; Liu *et al.* , 2021; Lopez-Alvis *et al.* , 2021), explore the dimensionality of geophysical data (Dokht Dolatabadi Esfahani *et al.* , 2021), and predict subsurface geological properties (Li and Misra, 2017).

Following Yin et al. (2021), the STFs of SCARDEC and YE2016 are resampled to 128 points as input size. Given that the longest STFs are approximately 100 s, the resulting sampling rates would be greater than 1 Hz. This reserves the frequency contents below 1 Hz for the STFs, which are relatively reliable by the SCARDEC method (Vallée and Douet, 2016; Yin et al., 2021). The amplitude of STFs is then normalized with the seismic moment to retain the shapes only (Meier et al., 2017; Yin et al., 2021). In this way, the normalized STF shapes likely do not contain direct information of earthquake size, and essentially only reflect the relative moment release with respect to the entire rupture process. However, there might be other features of the normalized shapes that are magnitude dependent and could be detected by the VAE approach. Unlike other STF normalization methods, such as stretching the amplitude and duration by ${M_0}^{-1/3}$ and ${M_0}^{-2/3}$ respectively (Houston, 2001; Vallée, 2013), the normalization adopted in this study leads to the loss of absolute time scale. Hence, interpretation of the results will be focused on temporal distribution of moment release relative to the earthquake's rupture process.

The VAE is constructed as follows: an input layer of 128 neurons, an encoder of two layers of 512 neurons each, a bottleneck of two neurons (latent representation), a decoder of two 512 neurons, and an output layer of 128 neurons (Figure 1). The use of two latent variables is key for the architecture as it determines the dimensionality of the latent space. Although using more latent variables can lead to better fit (refer to supporting infomation), two variables are used to capture the most essential features of STFs and allow direct visualization of the STF model in the latent space.

The loss function to train the VAE is defined as:

$$loss = \left\| \mathrm{STF}' - STF \right\| + KL \left[ \mathbb{N} \left( \mu_z, \sigma_z \right) - \mathbb{N} \left( 0, 1 \ \right) \right]$$

where the first term is the root mean square between the reconstructed and original STFs, and the second is the Kullback-Leibler divergence which measures the difference in probability density between the latent variable vector Z with mean $\mu$ and variance $\sigma$, and normal distribution. The Kullback-Leibler divergence essentially acts a regularizer of the latent space (Kingma and Welling, 2014). We use the Adam solver for network parameter optimization (Kingma and Ba, 2017).

The SCARDEC STFs are split in 80% for training and 20% for validation. The convergence of train and validation loss (Figure S1) ensures the model generalizability and warrants analysis of the entire data set altogether. An important sign for a well-trained VAE is the successful reconstruction of STFs for both SCARDEC and YE2016 (Figures 1b and 1c). Except for some complex events (e.g. 2000 Mw 8.1 New Ireland earthquake, 2006 Mw 8.3 Kuril earthquake, 2007 Mw 8.1 Peru earthquake), the reconstructed STFs capture the primary characteristics of most observed STFs, such as skewness and peakedness variations, demonstrating the learned low-dimensional latent variables are good representations of the high-dimensional STFs.

## The standard STF model

The VAE allows us to visualize the STFs orderly in both low- and high- dimensional spaces, which is important for evaluating their systematic variability. The encoder projects the STFs into a 2D latent space (Figure 2), whose affinity property ensures that similar STFs are located closely in the latent space (Figure S2). Because of the imposed regularizer on the latent variables, earthquake population in the latent space generally follows a normal distribution, i.e. approximately ~68% of earthquakes within the radius of 1 and 95% of earthquakes within the radius of 2. Based on these two properties, the most common STF shapes are mapped near the center, whereas the rare ones are mapped outwards.

To visualize the overall STF variations, we input virtual latent parameters at every 0.5 interval from -3.0 to 3.0 into the decoder to construct a set of synthetic STFs (Figure 2b). Because each of these STFs is constrained by real STFs near its locality in the latent space, they represent the generic variations of global earthquakes. Therefore, we call this synthetic collection as the standard STF model. It is noteworthy that the synthetic STFs are constrained with a different number of STFs, according to the population distribution of real STFs. Overall, the standard model exhibits three outstanding characteristics that vary continuously: number of peaks, skewness, and peakedness (Figures 2b and S3). For convenience of discussion, the model is divided into four quadrants based on the changes of characteristics:

$Q_1$: $Z_1>-0.5$, $Z_2>0.5$, $Q_2$: $Z_1<-0.5$, $Z_2>0$

$Q_3$: $Z_1<-0.5$, $Z_2<0$, $Q_4$: $Z_1>-0.5$, $Z_2<0.5$

Where $Z_1$ and $Z_2$ are the first and second latent variable, respectively. $Q_1$ represents the complex type with two or more subevents with varying relative size and timings. In comparison, events in $Q_2$ , $Q_3$ , and $Q_4$ are single peaked but negative-skewed (runaway), symmetric, and positive-skewed (long-tail) types, respectively. Overall, the one-peak types $Q_2$ -$Q_4$ account for 83% of global events (16% runaway, 15% symmetric, 52% long-tail), whereas the complex type in $Q_1$ accounts for 17%.

Skewness measures the relative duration of moment acceleration and deceleration phases. The long-tailed shapes suggest the rupture breaks away energetically but die away slowly. They have the largest population among all the types, consistent with pervasive energetic onsets of large earthquakes (Denolle, 2019). However, part of them, especially those with very long tails, could be due to artifacts from imperfect modeling of P wave coda (Vallée and Douet, 2016). The symmetric type suggests near equivalent acceleration and deceleration duration, which is often considered a generic STF shape in standard models (e.g. Tanioka and Ruff, 1997). Finally, the runaway type has a relatively weak onset, representing ruptures that culminate in the late rupture stage. This type of events is of particular interest, because they are misguided as small events at the beginning but their final magnitude is largely determined by the later phase. The runaway type is comparably populated as the symmetric type. Notice that while long-tailed shapes appear to be more typical over all, there seems to be a pattern shift to the negative $Z_1$ direction (runaway and symmetric) with increasing magnitude. This phenomenon will be discussed in the last section.

Peakedness, another characteristic revealed in the model, measures the temporal homogeneity of moment release. From the center to periphery, peak width decreases. The rounded peaks near the center suggests relatively homogenous moment release during the rupture, whereas the spiky peaks in the periphery suggest that a predominant amount of energy is released within a compact prime time relative to the entire rupture duration. One should note that the compactness is not in the sense of physical time scale, which is lost in normalization, but is relative to the earthquake's rupture process itself. For example, earthquakes with different moment release rates may have the same temporal homogeneity. The population distribution suggests that earthquakes with homogenous moment release is much more populated than the highly concentrated ones, reflecting the prevalence of homogenous faulting in nature.

## Earthquakes outside the norm

The model describes a comprehensive set of standard shapes that represent a majority of global earthquakes. However, some earthquakes cannot be adequately described by the model. The excursion is quantified by the misfit between the reconstructed and original STFs $\frac{\|\mathrm{STF}_{\mathrm{rec}}-\mathrm{STF}_{\mathrm{raw}}\|}{\|\mathrm{STF}_{\mathrm{raw}}\|}$. While the majority of the SCARDEC events have predominantly small misfits (Figure 3a), some have unusually high misfits, such as the 2006 M 7.7 Java tsunami earthquake, 2006 M 8.3 Kuril earthquake and 2007 M 8.1 Solomon tsunami earthquake (Figure S4). These events have complex STFs and are documented with unusual rupture characteristics (Ammon*et al.* , 2006, 2008; Furlong *et al.* , 2009). Hence, the events with high misfits represent a special class of unusual earthquakes outside the norm.

The complex events can be categorized according to their latent locality, i.e. the systematic ones in $Q_1$ and the individual ones in other quadrants. The high misfits observed in $Q_1$ indicate the actual shapes there are even more complicated than depicted in the model. These events have temporally separated subevents, representing ruptures of relatively distant asperities/faults or inter-event triggering. In comparison, the high-misfit events outside $Q_1$ are fit with simple one-peak shapes, yet exhibiting complex characteristics. They appear to be temporally more compact and generally "rougher". This could be interpreted as ruptures of spatially concentrated asperities and/or heterogeneous frictional properties along faults (Ye *et al.* , 2018).

Figure 3 shows that the complex events exhibits three intriguing characteristics: 1) they are shallower than 40 km; 2) they exist in all faulting environments; 3) many are located along the northern boundaries of the Australian plate and in Southeast Asia. Houston (2001) found that the complexity of events is generally higher in the top 40 km in global subduction zones. She attributed this phenomenon to heterogeneous interplate boundary regions. However, in our results, the complex events are found to exist in all different mechanisms, suggesting more universal depth-dependent rupture complexity. Applying cluster analysis to the SCARDEC data, Yin et al. (2021) also identified depth dependence of earthquake complexity. They proposed that variations of frictional properties with depth, such as slip weakening distance or other equivalent rupture parameters could play an important role in controlling rupture complexity. One should note that some complex shallow events might be caused by the artifacts of unmodelled seismic phases, such as depth phases (Vallée and Douet, 2016). However, Yin et al. (2021) observed that co-located shallow events have various degrees of complexity, indicating inaccuracy in the Green's function does not impact the overall observations. Moreover, to mitigate the structural effect, the SCARDEC method cuts the STFs after the last local maximum 40% of the absolute maximum.

Alternatively, we hypothesize that there could be more geometric and stress irregularities (e.g. faults and asperities) at shallow depths owing to low confining pressure and temperature. In a statistical perspective, the larger population of geometric and stress irregularities allows higher chance of triggering and accidental activation during rupture. This hypothesis is partly supported by the pervasiveness of complex events in the apparently complex fault systems, such as in the northern boundaries of the Australian plate and in Southeast Asia (Figure 3), although the causes for specific complex events could be case dependent.

## Discussion

### *Implications for earthquake rupture diversity*

The VAE condenses a large number of global earthquake observations into the standard STF model along with the information of population density, which unravels more diverse rupture characteristics than the mean shape from commonly used stacking methods. Complementary to the model, the reconstruction misfit quantifies the deviation of individual earthquakes and naturally measures the rupture uniqueness. These components taken together provide a panoramic view of earthquake rupture variability and showcase the extent that large earthquakes share common rupture characteristics.

Our observations, first of all, confirm that earthquakes with apparent simple rupture processes are predominant and that the extremely skewed or complex ones are rare. Around the model center with highest population density, the shapes are weakly skewed and gently peaked, representing relatively homogenous and apparent one-patch-like rupture processes. This is generally consistent with the simple mean shape reported by Meier et al. (2017). However, the model offers a much richer collection of standard shapes other than the simple mean. Beyond one standard deviation, for example, the shapes start to exhibit significant skewness and more complexity, reflecting increasingly irregular rupture processes. These irregular types comprise a non-negligible proportion of the entire earthquake population (e.g. 32% if counting those outside radius 1), which should be interpreted by more sophisticated rupture models.

The STF model derived by the VAE approach aims to quantify the first and second order features of global earthquakes' STFs, which is similar to the STF model by Meier et al (2017). However, the two models differ in some important aspects. For example, in addition to the median STF, Meier et al (2017) quantified the statistical fluctuations, which is found to be multiplicative and Gaussian-like. Their model considers a real STF as the median STF perturbed by random fluctuations at all frequencies. In comparison, our model produces smoother STFs and the high-frequency roughness of real STFs is assimilated in the misfit and viewed as part of earthquake complexity (Figures 1-3). Moreover, our model has two controlling parameters to reconstruct the STFs and take a misfit metric to measure the excursion, whereas the model of Meier et al. (2017) has controlling parameters as many as the fluctuation phases at all frequencies. These differences are essentially sourced from different decomposition schemes of real STFs resulted from the respective methods.

*Implications for earthquake early warning*

The diversity of temporal moment release patterns imposes a limit on magnitude determinism, i.e. the predictability of earthquake size before the rupture is complete. A near isosceles triangular shape averaged from all STFs suggests that approximately half the duration is required to predict final magnitude (Meier et al., 2017). In addition, many symmetric events observed in the model exhibit a low-amplitude onset acceleration, which may also lead to magnitude underestimate in early warning. For the runaway events, the early amplitude is particularly small and long and the peak moment rate arrives much later. This runaway behavior could be caused by dynamic weakening mechanisms during the rupture development , such as flash heating and thermal pressurization, resulting in the break of strong asperities in the later rupture stage (Denolle et al., 2015). Alternatively, it could be also caused by triggering a later large asperity by an early small asperity. In this case, both ruptures are so close in time that the moment release appears to be one peak. More generally, triggering among asperities with different sizes and spatial separations can result in other types of events as well. Recent discoveries of similar initial waveforms between large and small earthquakes imply that whether or not a small event can develop into a big one could be in part a stochastic result (Okuda and Ide, 2018; Ide, 2019). Hence, this type of events poses a greater challenge for early warning.

Although STFs predicted by the Brune and Haskell models (Haskell, 1964; Brune, 1970) as well as those empirically derived tend to emphasize the importance of symmetric and long-tail STFs (Tanioka and Ruff, 1997), our results show that the population of the runaway type is actually comparable to that of the symmetric type. The examples of large runaway events include the 1996 Mw 7.7 and 2001 Mw 7.6 Peru, 2010 Mw 8.8 Chile, and 2011 Mw 7.3 Honshu earthquakes (Figure S4). In addition to the runaway type, complex events represented in $Q_1$have subevents with unknown relative size and timing, which can further confuse early warning systems. It seems that there is no effective way to diagnose the event type when the rupture is developing, making early magnitude estimation more challenging. Recent studies also show that that the absolute duration can vary significantly even for earthquakes with similar magnitudes (Vallée, 2013; Sallarès and Ranero, 2019), which further decreases magnitude predictability beyond the discussed STF shape diversity. Therefore, early estimates of earthquake magnitude would expectedly often excurse, even though it could be partly inferred (Melgar and Hayes, 2019).

*Potentials for revealing earthquake mechanics*

An important question in earthquake science is whether or not rupture processes are magnitude-dependent (Meier et al., 2017; Ye et al., 2018; Melgar and Hayes, 2019; Renou et al., 2019). Figure 2a shows stark contrast in the numbers of M>8 events in $Z_1>0$ and $Z_1<0$ quadrants, implying a plausible preferential rupture mode for M>8 events. In fact, we observe that the largest earthquakes seem to shift systematically to the negative $Z_1$ direction (Figure 4). We estimate the statistical significance of this trend by bootstrap tests. To reduce the impact of scarcity of large-magnitude events, in each test, 100 events are randomly drawn in each magnitude bin (Figure 4a and b) for calculation of Spearman correlation and p value. For bins with less than 100 events, all the events in the bins are used. This procedure is repeated 1,000 times. The results show that $Z_1$ has correlation$0.20 \pm 0.03$ with magnitude and p value $10^{-8\pm2}$, suggesting a statistically significant pattern shift along the $Z_1$ direction (Figure 4). In contrast, $Z_2$has correlation $0.067 \pm 0.03$ with magnitude and p value$10^{-1.3\pm0.8}$, suggesting negligible change along the $Z_2$ direction. This magnitude-dependent $Z_1$ distribution implies that the largest earthquakes seemingly prefer to begin with small events (symmetric or run-away types) rather than release most of the energy in the early stage (long-tail type). An admissible explanation is that a relatively high level of rupture momentum and dynamic weakening is likely needed to activate and break unusually large and/or strong asperities.

More generally, the encoder-decoder system provides an effective tool to investigate potential pattern variations with source parameters and thus could offer useful insights into the physics of rupture processes. It also provides a convenient tool to evaluate the generality and peculiarity of particular events in the context of historical observations in a uniform framework. Our study illustrates that generative unsupervised machine learning could be powerful in uncovering underlying collective patterns of high-dimensional seismic data.


## Acknowledgements

I would like to thank the editor Germán Prieto, Jean-Paul Ampuero and an anonymous reviewer for their constructive comments. This work has benefited from discussion with Jiuxun Yin, Hiroo Kanamori, Men-Andrin Meier, Han Yue, and Lingling Ye. I thank Martin Vallee and Lingling Ye for providing their source time function databases and thank Xin Cui for help in the bootstrapping tests. This work is by supported by the research startup fund from USTC (Grant No. KY2080000079).


## Data Availability

The SCARDEC database is available at http://scardec.projects.sismo.ipgp.fr/ (last accessed on September 3, 2021). The STFs of megathrust earthquakes can be accessed from the supplementary material in Ye et al. (2016) (doi.org/10.1002/2015JB012426, last accessed on September 3, 2021).

## Author contributions

Z. L. conceive the idea, analyze the data and write the manuscript.

## Competing interests

The author declares no competing interests.

## References


Ammon, C. J. (2005). Rupture Process of the 2004 Sumatra-Andaman Earthquake, *Science* **308** , no. 5725, 1133–1139, doi: 10.1126/science.1112260.

Ammon, C. J., H. Kanamori, and T. Lay (2008). A great earthquake doublet and seismic stress transfer cycle in the central Kuril islands,*Nature* **451** , no. 7178, 561–565, doi: 10.1038/nature06521.

Ammon, C. J., H. Kanamori, T. Lay, and A. A. Velasco (2006). The 17 July 2006 Java tsunami earthquake, *Geophys. Res. Lett.* **33** , no. 24, doi: 10.1029/2006GL028005.

Brune, J. N. (1970). Tectonic stress and the spectra of seismic shear waves from earthquakes, *J. Geophys. Res. 1896-1977* **75** , no. 26, 4997–5009, doi: 10.1029/JB075i026p04997.

Cheng, X., and K. Jiang (2020). Crustal model in eastern Qinghai-Tibet plateau and western Yangtze craton based on conditional variational autoencoder, *Phys. Earth Planet. Inter.* **309** , 106584, doi: 10.1016/j.pepi.2020.106584.

Denolle, M. A. (2019). Energetic Onset of Earthquakes, *Geophys. Res. Lett.* **46** , no. 5, 2458–2466, doi: 10.1029/2018GL080687.

Denolle, M. A., W. Fan, and P. M. Shearer (2015). Dynamics of the 2015 M7.8 Nepal earthquake, *Geophys. Res. Lett.* **42** , no. 18, 7467–7475, doi: 10.1002/2015GL065336.

Dokht Dolatabadi Esfahani, R., K. Vogel, F. Cotton, M. Ohrnberger, F. Scherbaum, and M. Kriegerowski (2021). Exploring the Dimensionality of Ground-Motion Data by Applying Autoencoder Techniques, *Bull. Seismol. Soc. Am.* , doi: 10.1785/0120200285.

Duputel, Z., V. C. Tsai, L. Rivera, and H. Kanamori (2013). Using centroid time-delays to characterize source durations and identify earthquakes with unique characteristics, *Earth Planet. Sci. Lett.***374** , 92–100, doi: 10.1016/j.epsl.2013.05.024.

Furlong, K. P., T. Lay, and C. J. Ammon (2009). A Great Earthquake Rupture Across a Rapidly Evolving Three-Plate Boundary, *Science***324** , no. 5924, 226–229, doi: 10.1126/science.1167476.

Haskell, N. A. (1964). Total energy and energy spectral density of elastic wave radiation from propagating faults, *Bull. Seismol. Soc. Am.* **54** , no. 6A, 1811–1841.

Houston, H. (2001). Influence of depth, focal mechanism, and tectonic setting on the shape and duration of earthquake source time functions,*J. Geophys. Res. Solid Earth* **106** , no. B6, 11137–11150, doi: 10.1029/2000JB900468.

Houston, H., and J. E. Vidale (1994). The Temporal Distribution of Seismic Radiation During Deep Earthquake Rupture, *Science***265** , no. 5173, 771–774, doi: 10.1126/science.265.5173.771.

Ide, S. (2019). Frequent observations of identical onsets of large and small earthquakes, 7772, *Nature* **573** , no. 7772, 112–116, doi: 10.1038/s41586-019-1508-5.

Kingma, D. P., and J. Ba (2017). Adam: A Method for Stochastic Optimization, *ArXiv14126980 Cs* .

Kingma, D. P., and M. Welling (2014). Auto-Encoding Variational Bayes, in *Proceedings of the International Conference on Learning Representations (ICLR)* .

Li, H., and S. Misra (2017). Prediction of Subsurface NMR T2 Distributions in a Shale Petroleum System Using Variational Autoencoder-Based Neural Networks, *IEEE Geosci. Remote Sens. Lett.* **14** , no. 12, 2395–2397, doi: 10.1109/LGRS.2017.2766130.

Liu, M., D. Grana, and L. P. de Figueiredo (2021). Uncertainty quantification in stochastic inversion with dimensionality reduction using variational autoencoder, *GEOPHYSICS* , 1–65, doi: 10.1190/geo2021-0138.1.

Lopez-Alvis, J., E. Laloy, F. Nguyen, and T. Hermans (2021). Deep generative models in inversion: The impact of the generator's nonlinearity and development of a new approach based on a variational autoencoder, *Comput. Geosci.* **152** , 104762, doi: 10.1016/j.cageo.2021.104762.

Meier, M.-A., J. P. Ampuero, and T. H. Heaton (2017). The hidden simplicity of subduction megathrust earthquakes, *Science***357** , no. 6357, 1277–1281, doi: 10.1126/science.aan5643.

Melgar, D., and G. P. Hayes (2019). Characterizing large earthquakes before rupture is complete, *Sci. Adv.* **5** , no. 5, eaav2032, doi: 10.1126/sciadv.aav2032.

Meng, L., J.-P. Ampuero, J. Stock, Z. Duputel, Y. Luo, and V. C. Tsai (2012). Earthquake in a Maze: Compressional Rupture Branching During the 2012 Mw 8.6 Sumatra Earthquake, *Science* **337** , no. 6095, 724–726, doi: 10.1126/science.1224030.

Okuda, T., and S. Ide (2018). Hierarchical rupture growth evidenced by the initial seismic waveforms, 1, *Nat. Commun.* **9** , no. 1, 3714, doi: 10.1038/s41467-018-06168-3.

Persh, S. E., and H. Houston (2004). Deep earthquake rupture histories determined by global stacking of broadband P waveforms, *J. Geophys. Res. Solid Earth* **109** , no. B4, doi: https://doi.org/10.1029/2003JB002762.

Renou, J., M. Vallée, and P. Dublanchet (2019). How Does Seismic Rupture Accelerate? Observational Insights From Earthquake Source Time Functions, *J. Geophys. Res. Solid Earth* **124** , no. 8, 8942–8952, doi: 10.1029/2019JB018045.

Ross, Z. E., B. Idini, Z. Jia, O. L. Stephenson, M. Zhong, X. Wang, Z. Zhan, M. Simons, E. J. Fielding, S.-H. Yun, *et al.* (2019). Hierarchical interlocked orthogonal faulting in the 2019 Ridgecrest earthquake sequence, *Science* **366** , no. 6463, 346–351, doi: 10.1126/science.aaz0109.

Sallarès, V., and C. R. Ranero (2019). Upper-plate rigidity determines depth-varying rupture behaviour of megathrust earthquakes, *Nature***576** , no. 7785, 96–101, doi: 10.1038/s41586-019-1784-0.

Shearer, P. M., G. A. Prieto, and E. Hauksson (2006). Comprehensive analysis of earthquake source spectra in southern California, *J. Geophys. Res. Solid Earth* **111** , no. B6, doi: 10.1029/2005JB003979.

Tanioka, Y., and L. J. Ruff (1997). Source Time Functions,*Seismol. Res. Lett.* **68** , no. 3, 386–400, doi: 10.1785/gssrl.68.3.386.

Vallée, M. (2013). Source time function properties indicate a strain drop independent of earthquake depth and magnitude, *Nat. Commun.***4** , no. 1, 2606, doi: 10.1038/ncomms3606.

Vallée, M., and V. Douet (2016). A new database of source time functions (STFs) extracted from the SCARDEC method, *Phys. Earth Planet. Inter.* **257** , 149–157, doi: 10.1016/j.pepi.2016.05.012.

Ye, L., H. Kanamori, and T. Lay (2018). Global variations of large megathrust earthquake rupture characteristics, *Sci. Adv.***4** , no. 3, eaao4915, doi: 10.1126/sciadv.aao4915.

Ye, L., T. Lay, H. Kanamori, and L. Rivera (2016). Rupture characteristics of major and great ( $M_w$ [?] 7.0) megathrust earthquakes from 1990 to 2015: 1. Source parameter scaling relationships, *J. Geophys. Res. Solid Earth* **121** , no. 2, 826–844, doi: 10.1002/2015JB012426.

Yin, J., Z. Li, and M. A. Denolle (2021). Source Time Function Clustering Reveals Patterns in Earthquake Dynamics, *Seismol. Res. Lett.* **92** , no. 4, 2343–2353.

**Figures**

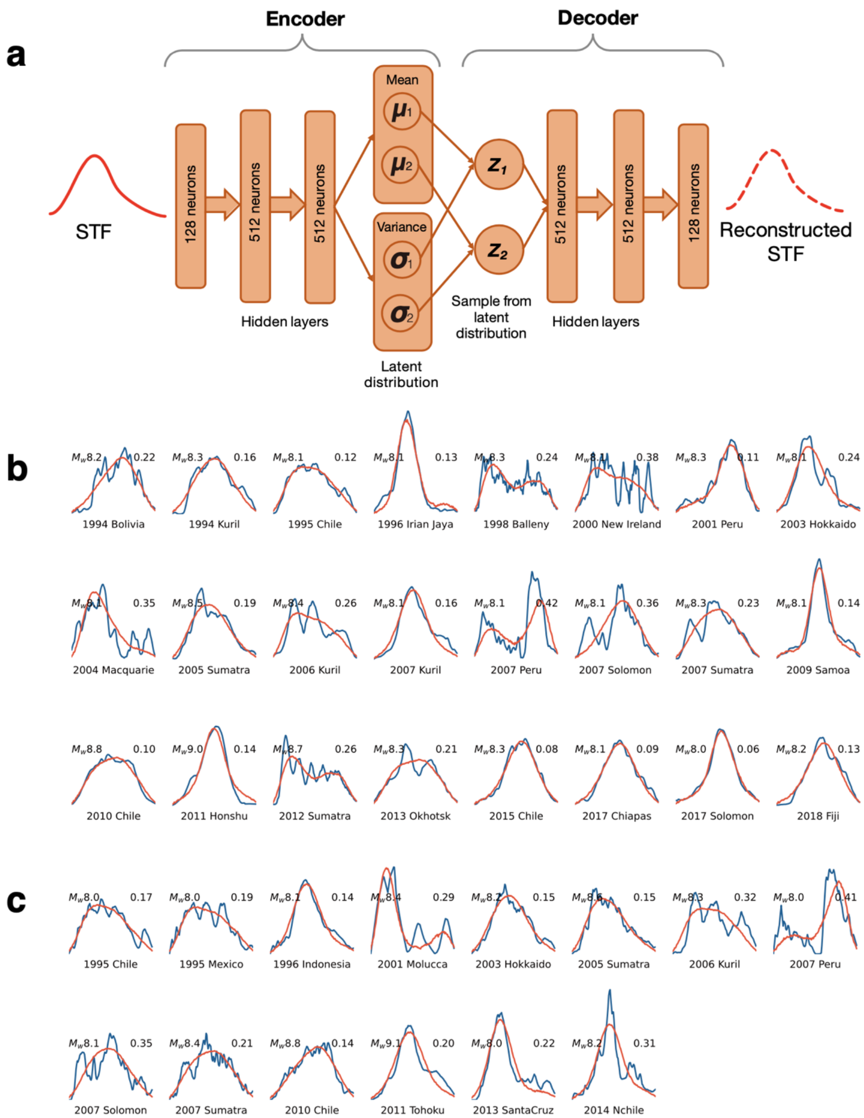


**Figure 1. Variational autoencoder (VAE) for earthquake source time functions (STFs).** a. VAE architecture. Both of the decoder and encoder consist of two fully connected layers with 512 neurons each. The bottleneck consists of two latent variables constrained to follow normal distribution. b. Original STFs (blue) and VAE reconstructed STFs (red) from SCARDEC. The numbers in the top right mark the misfits. c. Same as b but for the STF database of Ye et al. (2016) (referred to as YE2016 thereinafter).

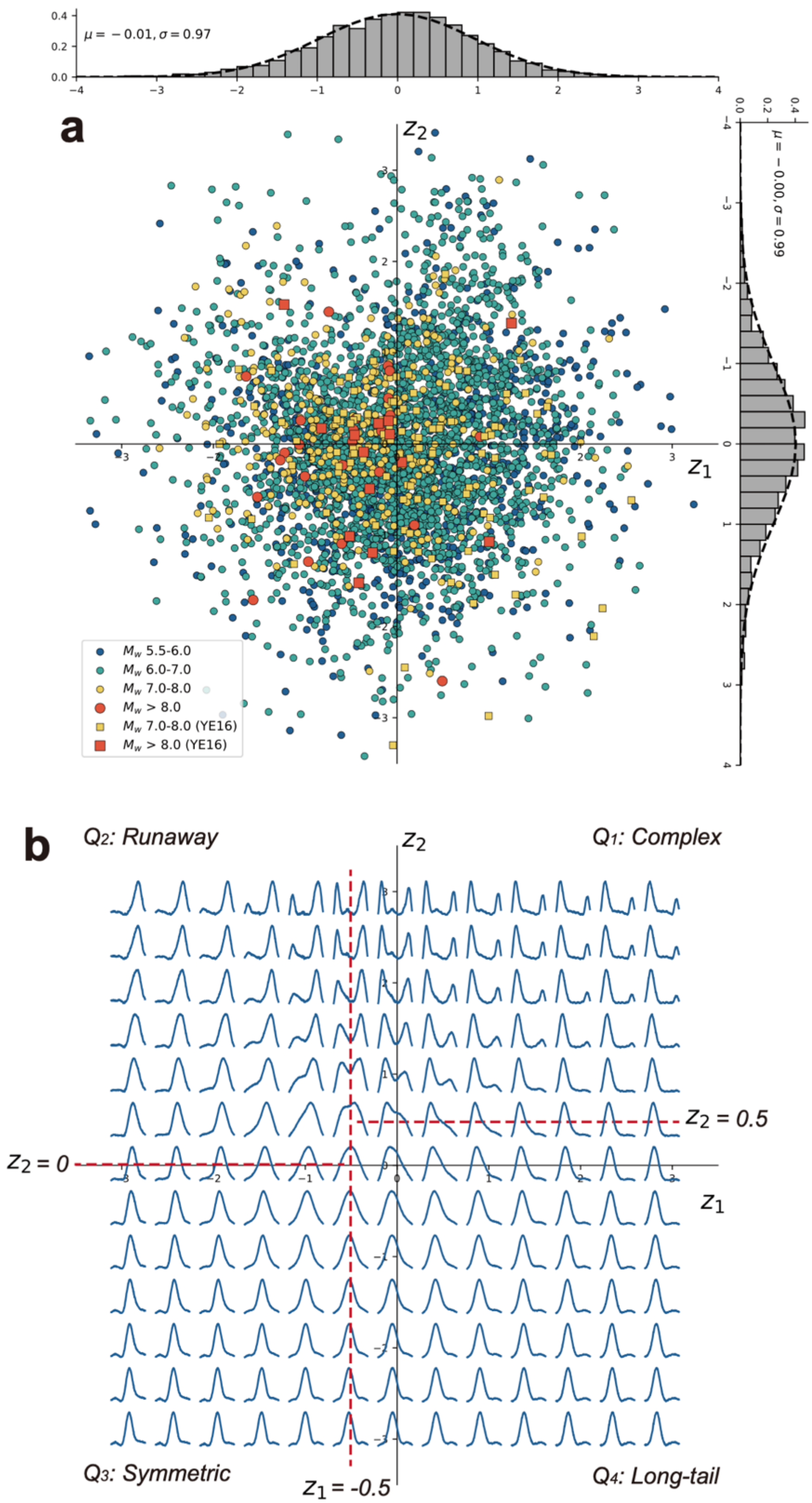

a
$\mu = -0.01, \sigma = 0.97$
$\mu = -0.00, \sigma = 0.99$
$z_2$
$z_1$
$M_w$ 5.5-6.0
$M_w$ 6.0-7.0
$M_w$ 7.0-8.0
$M_w$ > 8.0
$M_w$ 7.0-8.0 (YE16)
$M_w$ > 8.0 (YE16)
b
Q2: Runaway
Q1: Complex
$z_2$
$z_2 = 0.5$
$z_2 = 0$
$z_1$
Q3: Symmetric
$z_1 = -0.5$
Q4: Long-tail

**Figure 2. The latent representation and the standard model of STFs.** a. Low-dimensional latent representations of SCARDEC (dots) and YE2016 (squares) STFs. The population density in both $Z_1$ and $Z_2$ follows normal distribution. b. The standard STF model reconstructed from virtual latent values. The model shows systematic variations of STFs: complex type in $Q_1$ , runaway type in $Q_2$ , symmetric type in $Q_3$ , and long-tail type in $Q_4$ .

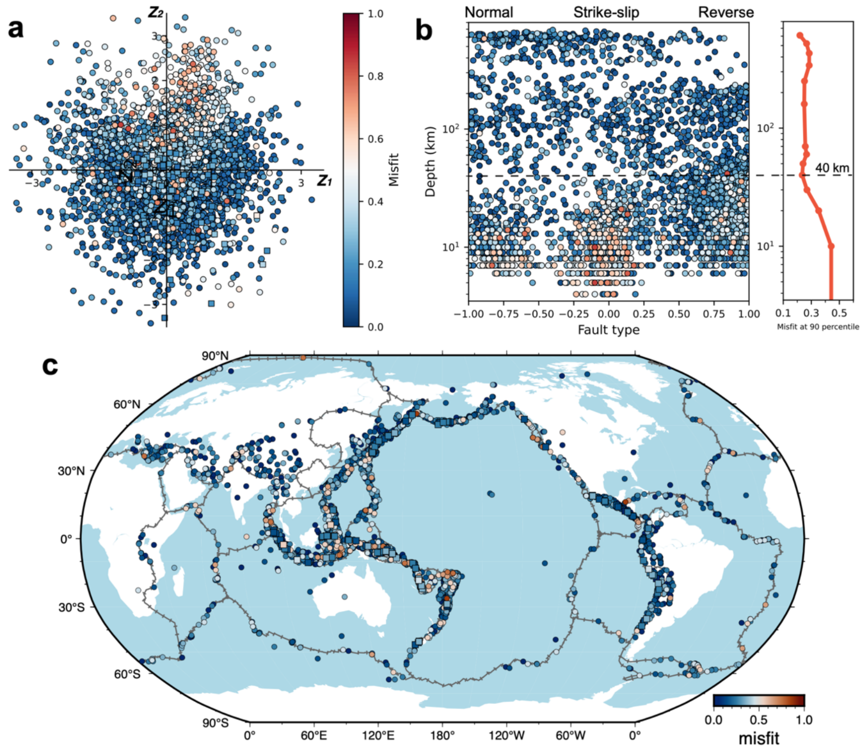


**Figure 3. Reconstruction misfit as a proxy of unusual earthquakes.** a. Reconstruction misfits of all the SCARDEC (dots) and YE2016 (squares) events in latent space. Note that most high-misfits are located in $Q_1$ and some are in other quadrants. b. Reconstruction misfit as a function of earthquake depth and focal mechanisms. The definition of fault type follows Shearer et al. (2006). On the right is the median misfit across depth. The depth at 40 km marks the change point of earthquake complexity. c. Geographic distribution of reconstruction misfit of global earthquakes. Note that the high-misfits are predominantly located in the northern boundaries of the Australian plate and Southeast Asia.

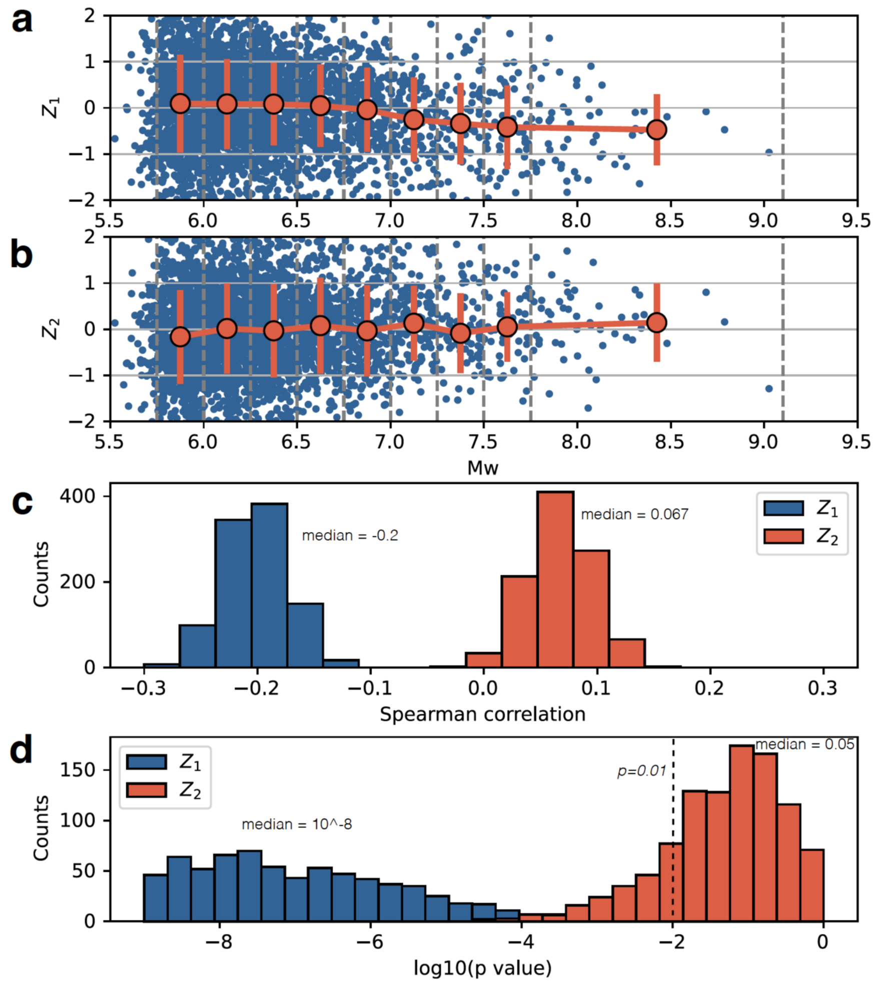


**Figure 4. Dependencies of latent variables $\mathbf{Z_1}$and $\mathbf{Z_2}$ on magnitude.** a. Blue dots represent $Z_1$ of individual earthquakes. Red dots and bars represent the mean and standard deviation in each magnitude bin bracketed by dashed gray lines. b. Similar symbol representation as in a but for $Z_2$. c. Histograms of Spearman correlations between $Z_1$, $Z_2$ and magnitude from bootstrapping tests. d. Histograms of p values for hypothesis test in which null hypothesis is that $Z_1$, $Z_2$ are uncorrelated with magnitude. In each test, 100 events are randomly selected in each magnitude bin (for bins with less than 100 events, all within the bins are used) to calculate the correlation and p-value, which is repeated 1,000 times.

**Hosted file**

`li_stfspectrum_supp_revised.docx` available at https://authorea.com/users/538168/articles/607911-a-generic-model-of-global-earthquake-rupture-characteristics-revealed-by-machine-learning

# A generic model of global earthquake rupture characteristics revealed by machine learning

**Zefeng Li**[1,2*]

*1. Laboratory of Seismology and Physics of Earth's Interior, School of Earth and Space Sciences, University of Science and Technology of China, Hefei, China*

*2. Mengcheng National Geophysical Observatory, University of Science and Technology of China, Mengcheng, China*

*Manuscript submitted to GRL*

*Corresponding author: Zefeng Li (zefengli@ustc.edu.cn)

**Highlights:**

1. A generic model of characteristic source time functions is derived from global earthquake observations using machine learning.
2. The model presents a panoptic view of the similarity and the diversity in the rupture processes of large earthquakes.
3. The diversity of moment release patterns, together with absolute duration variability, imposes a limit on magnitude predictability in early warning.

**Abstract**

Rupture processes of global large earthquakes have been observed to exhibit great variability, whereas recent studies suggest that the average rupture behavior could be unexpectedly simple. To what extent do large earthquakes share common rupture characteristics? Here we use a machine learning algorithm to derive a generic model of global earthquake source time functions. The model indicates that simple and homogeneous ruptures are pervasive whereas complex and irregular ruptures are relatively rare. Despite the standard long-tail and near-symmetric moment release processes, the model reveals two special rupture types: runaway earthquakes with weak growing phases and relatively abrupt termination, and complex earthquakes with all faulting mechanisms but mostly shallow origins (<40 km). The diversity of temporal moment release patterns imposes a limit on magnitude predictability in earthquake early warning. Our results present a panoptic view on the collective similarity and diversity in the rupture processes of global large earthquakes.

**Plain language summary**

Over the past decades, seismologists have observed great variability in the rupture processes of many large earthquakes. However, some recent studies suggest that the average rupture behavior could be unexpectedly simple. Can the average behavior be representative of most earthquakes? To what extent do large earthquakes share common rupture characteristics? Here we use machine learning to derive a panoptic picture, i.e. a generic model of source time functions, for global earthquakes. The model shows that simple and homogeneous ruptures are pervasive whereas complex and irregular ruptures are relatively rare. Besides, it reveals two special rupture types: runaway earthquakes with weak initial phases, and complex earthquakes with all faulting mechanisms but mostly shallow origins (<40 km). Our results present a panoptic view on the collective similarity and diversity in the rupture processes of global large earthquakes, which affects how well we can predict earthquake magnitude in earthquake early warning.

## Introduction

Large earthquakes start, propagate, and terminate in diverse manners owing to complex interplay between rupture dynamics and fault properties. Over the past decades, observations of large earthquake rupture processes have shown various degrees of peculiarity (Ammon, 2005; Ammon *et al.*, 2006; Meng *et al.*, 2012; Ross *et al.*, 2019), suggesting that each large earthquake probably has its own unique characteristics. However, understanding the general physical laws that govern earthquake phenomena requires derivation of the underlying patterns from the seemingly diverse behaviors (Houston and Vidale, 1994; Vallée, 2013; Meier *et al.*, 2017; Denolle, 2019). The average behaviors, often obtained by stacking a large set of seismological data, tend to show relatively simple characteristics, implying common similarity hidden behind the diverse ruptures (Houston and Vidale, 1994; Meier *et al.*, 2017). The distinct emphases on collective rupture peculiarity and similarity raises a critical question: to what extent do large earthquakes share common rupture characteristics? Answering this question calls for a panoptic view of the variability in the rupture processes of global earthquakes.

Earthquake source time functions (STFs) describes the history of seismic moment release during rupture. As an important observation constraining on the source processes, STFs have been routinely extracted from seismograms for large earthquakes. However, because of the high-dimensionality and great variations of amplitude and duration (Tanioka and Ruff, 1997; Duputel *et al.*, 2013; Vallée, 2013), STFs cannot be compared directly. Hence, comparison is often performed on individual STF properties such as duration, peak amplitude, peaks and skewness (Houston, 2001; Persh and Houston, 2004), as well as other derived parameters, such as scaled energy (Denolle, 2019) and relative radiated energy efficiency (Ye *et al.*, 2018). Although these individual properties constrain specific aspects of earthquake ruptures, it remains challenging to examine the variability of overall moment release processes.

Here we employ a machine learning algorithm, called variational autoencoder (VAE), to illuminate the systematic variability of STF shapes among global earthquakes (Figure 1). We train a VAE with normalized STFs of 3675 $M>5.5$ global earthquakes from 1992 to 2019 (SCARDEC database, Vallée & Douet, 2016). This trained VAE is applied to another independent database of 112 STF of M>7.0 megathrust earthquakes (Ye *et al.*, 2016; referred to as YE2016), to validate its generalization capability. With the VAE, we derive a standard STF model that contains a systematic set of characteristic shapes accompanied by corresponding earthquake population density. The model exhibits a broad range of rupture characteristics for global earthquakes and sheds light on special classes of earthquakes that have not received sufficient attention before. Moreover, the deviation of individual earthquakes from the standard model is measured by the reconstruction misfit. Hence, large reconstruction misfits naturally detect earthquakes outside the norm, i.e. earthquakes with unusual rupture processes.

**VAE for STFs**

VAE is widely used in signal and image processing to uncover the intrinsic structure of a large data set (Kingma and Welling, 2014). It consists of an encoder to compress the high-dimensional data into a low-dimensional latent representation and a decoder to reconstruct the high-dimensional data from the latent representation (Figure 1). The bottleneck architecture forces the algorithm to learn the key data characteristics and discards the noise in individual samples. After training, the VAE can take input of virtual latent values (a set of parameters in the bottleneck that encode original data) from a random normal distribution to generate synthetic data constrained by real observations, and therefore belongs to generative learning methods. In geophysics, VAE has been recently used to speed up geophysical inversion (Cheng and Jiang, 2020; Liu *et al.*, 2021; Lopez-Alvis *et al.*, 2021), explore the dimensionality of geophysical data (Dokht Dolatabadi Esfahani *et al.*, 2021), and predict subsurface geological properties (Li and Misra, 2017).

Following Yin et al. (2021), the STFs of SCARDEC and YE2016 are resampled to 128 points as input size. Given that the longest STFs are approximately 100 s, the resulting sampling rates would be greater than 1 Hz. This reserves the frequency contents below 1 Hz for the STFs, which are relatively reliable by the SCARDEC method (Vallée and Douet, 2016; Yin et al., 2021). The amplitude of STFs is then normalized with the seismic moment to retain the shapes only (Meier et al., 2017; Yin et al., 2021). In this way, the normalized STF shapes likely do not contain direct information of earthquake size, and essentially only reflect the relative moment release with respect to the entire rupture process. However, there might be other features of the normalized shapes that are magnitude dependent and could be detected by the VAE approach. Unlike other STF normalization methods, such as stretching the amplitude and duration by $\mathrm{M_0}^{-1/3}$ and $\mathrm{M_0}^{-2/3}$ respectively (Houston, 2001; Vallée, 2013), the normalization adopted in this study leads to the loss of absolute time scale. Hence, interpretation of the results will be focused on temporal distribution of moment release relative to the earthquake's rupture process.

The VAE is constructed as follows: an input layer of 128 neurons, an encoder of two layers of 512 neurons each, a bottleneck of two neurons (latent representation), a decoder of two 512 neurons, and an output layer of 128 neurons (Figure 1). The use of two latent variables is key for the architecture as it determines the dimensionality of the latent space. Although using more latent variables can lead to better fit (refer to supporting infomation), two variables are used to capture the most essential features of STFs and allow direct visualization of the STF model in the latent space.

The loss function to train the VAE is defined as:

$$loss = \|STF' - STF\| + KL[\mathbb{N}(\mu_z, \sigma_z) - \mathbb{N}(0,1\ )]$$

where the first term is the root mean square between the reconstructed and original STFs, and the second is the Kullback-Leibler divergence which measures the difference in probability density between the latent variable vector $\boldsymbol{Z}$ with mean $\boldsymbol{\mu}$ and variance $\boldsymbol{\sigma}$, and normal distribution. The Kullback-Leibler divergence essentially acts a regularizer of the latent space (Kingma and Welling, 2014). We use the Adam solver for network parameter optimization (Kingma and Ba, 2017).

The SCARDEC STFs are split in 80% for training and 20% for validation. The convergence of train and validation loss (Figure S1) ensures the model generalizability and warrants analysis of the entire data set altogether. An important sign for a well-trained VAE is the successful reconstruction of STFs for both SCARDEC and YE2016 (Figures 1b and 1c).

Except for some complex events (e.g. 2000 Mw 8.1 New Ireland earthquake, 2006 Mw 8.3 Kuril earthquake, 2007 Mw 8.1 Peru earthquake), the reconstructed STFs capture the primary characteristics of most observed STFs, such as skewness and peakedness variations, demonstrating the learned low-dimensional latent variables are good representations of the high-dimensional STFs.

**The standard STF model**

The VAE allows us to visualize the STFs orderly in both low- and high- dimensional spaces, which is important for evaluating their systematic variability. The encoder projects the STFs into a 2D latent space (Figure 2), whose affinity property ensures that similar STFs are located closely in the latent space (Figure S2). Because of the imposed regularizer on the latent variables, earthquake population in the latent space generally follows a normal distribution, i.e. approximately ~68% of earthquakes within the radius of 1 and 95% of earthquakes within the radius of 2. Based on these two properties, the most common STF shapes are mapped near the center, whereas the rare ones are mapped outwards.

To visualize the overall STF variations, we input virtual latent parameters at every 0.5 interval from -3.0 to 3.0 into the decoder to construct a set of synthetic STFs (Figure 2b). Because each of these STFs is constrained by real STFs near its locality in the latent space, they represent the generic variations of global earthquakes. Therefore, we call this synthetic collection as the standard STF model. It is noteworthy that the synthetic STFs are constrained with a different number of STFs, according to the population distribution of real STFs. Overall, the standard model exhibits three outstanding characteristics that vary continuously: number of peaks, skewness, and peakedness (Figures 2b and S3). For convenience of discussion, the model is divided into four quadrants based on the changes of characteristics:

$$Q_1: Z_1>-0.5,\ Z_2>0.5, \quad Q_2: Z_1<-0.5,\ Z_2>0$$

$$Q_3: Z_1<-0.5,\ Z_2<0, \quad Q_4: Z_1>-0.5,\ Z_2<0.5$$

Where $Z_1$ and $Z_2$ are the first and second latent variable, respectively. $Q_1$ represents the complex type with two or more subevents with varying relative size and timings. In comparison, events in $Q_2$, $Q_3$, and $Q_4$ are single peaked but negative-skewed (runaway), symmetric, and positive-skewed (long-tail) types, respectively. Overall, the one-peak types $Q_2$-$Q_4$ account for 83% of global events (16% runaway, 15% symmetric, 52% long-tail), whereas the complex type in $Q_1$ accounts for 17%.

Skewness measures the relative duration of moment acceleration and deceleration phases. The long-tailed shapes suggest the rupture breaks away energetically but die away slowly. They have the largest population among all the types, consistent with pervasive energetic onsets of large earthquakes (Denolle, 2019). However, part of them, especially those with very long tails, could be due to artifacts from imperfect modeling of P wave coda (Vallée and Douet, 2016). The symmetric type suggests near equivalent acceleration and deceleration duration, which is often considered a generic STF shape in standard models (e.g. Tanioka and Ruff, 1997). Finally, the runaway type has a relatively weak onset, representing ruptures that culminate in the late rupture stage. This type of events is of particular interest, because they are misguided as small events at the beginning but their final magnitude is largely determined by the later phase. The runaway type is comparably populated as the symmetric type. Notice that while long-tailed shapes appear to be more typical over all, there seems to be a pattern shift to the negative $Z_1$ direction (runaway and symmetric) with increasing magnitude. This phenomenon will be discussed in the last section.

Peakedness, another characteristic revealed in the model, measures the temporal homogeneity of moment release. From the center to periphery, peak width decreases. The rounded peaks near the center suggests relatively homogenous moment release during the rupture, whereas the spiky peaks in the periphery suggest that a predominant amount of energy is released within a compact prime time relative to the entire rupture duration. One should note that the compactness is not in the sense of physical time scale, which is lost in normalization, but is relative to the earthquake's rupture process itself. For example, earthquakes with different moment release rates may have the same temporal homogeneity. The population distribution suggests that earthquakes with homogenous moment release is much more populated than the highly concentrated ones, reflecting the prevalence of homogenous faulting in nature.

**Earthquakes outside the norm**

The model describes a comprehensive set of standard shapes that represent a majority of global earthquakes. However, some earthquakes cannot be adequately described by the model. The excursion is quantified by the misfit between the reconstructed and original STFs $\frac{\|STF_{rec}-STF_{raw}\|}{\|STF_{raw}\|}$. While the majority of the SCARDEC events have predominantly small misfits (Figure 3a), some have unusually high misfits, such as the 2006 M 7.7 Java tsunami earthquake, 2006 M 8.3 Kuril earthquake and 2007 M 8.1 Solomon tsunami earthquake (Figure S4). These events have complex STFs and are documented with unusual rupture characteristics (Ammon *et al.*, 2006, 2008; Furlong *et al.*, 2009). Hence, the events with high misfits represent a special class of unusual earthquakes outside the norm.

The complex events can be categorized according to their latent locality, i.e. the systematic ones in $Q_I$ and the individual ones in other quadrants. The high misfits observed in $Q_I$ indicate the actual shapes there are even more complicated than depicted in the model. These events have temporally separated subevents, representing ruptures of relatively distant asperities/faults or inter-event triggering. In comparison, the high-misfit events outside $Q_I$ are fit with simple one-peak shapes, yet exhibiting complex characteristics. They appear to be temporally more compact and generally "rougher". This could be interpreted as ruptures of spatially concentrated asperities and/or heterogeneous frictional properties along faults (Ye *et al.*, 2018).

Figure 3 shows that the complex events exhibits three intriguing characteristics: 1) they are shallower than 40 km; 2) they exist in all faulting environments; 3) many are located along the northern boundaries of the Australian plate and in Southeast Asia. Houston (2001) found that the complexity of events is generally higher in the top 40 km in global subduction zones. She attributed this phenomenon to heterogeneous interplate boundary regions. However, in our results, the complex events are found to exist in all different mechanisms, suggesting more universal depth-dependent rupture complexity. Applying cluster analysis to the SCARDEC data, Yin et al. (2021) also identified depth dependence of earthquake complexity. They proposed that variations of frictional properties with depth, such as slip weakening distance or other equivalent rupture parameters could play an important role in controlling rupture complexity. One should note that some complex shallow events might be caused by the artifacts of unmodelled seismic phases, such as depth phases (Vallée and Douet, 2016). However, Yin et al. (2021) observed that co-located shallow events have various degrees of complexity, indicating inaccuracy in the Green's function does not impact the overall observations. Moreover, to mitigate the structural effect, the SCARDEC method cuts the STFs after the last local maximum 40% of the absolute maximum.

Alternatively, we hypothesize that there could be more geometric and stress irregularities (e.g. faults and asperities) at shallow depths owing to low confining pressure and temperature. In a statistical perspective, the larger population of geometric and stress irregularities allows higher chance of triggering and accidental activation during rupture. This hypothesis is partly supported by the pervasiveness of complex events in the apparently complex fault systems, such as in the northern boundaries of the Australian plate and in Southeast Asia (Figure 3), although the causes for specific complex events could be case dependent.

## Discussion

*Implications for earthquake rupture diversity*

The VAE condenses a large number of global earthquake observations into the standard STF model along with the information of population density, which unravels more diverse rupture characteristics than the mean shape from commonly used stacking methods. Complementary to the model, the reconstruction misfit quantifies the deviation of individual earthquakes and naturally measures the rupture uniqueness. These components taken together provide a panoramic view of earthquake rupture variability and showcase the extent that large earthquakes share common rupture characteristics.

Our observations, first of all, confirm that earthquakes with apparent simple rupture processes are predominant and that the extremely skewed or complex ones are rare. Around the model center with highest population density, the shapes are weakly skewed and gently peaked, representing relatively homogenous and apparent one-patch-like rupture processes. This is generally consistent with the simple mean shape reported by Meier et al. (2017). However, the model offers a much richer collection of standard shapes other than the simple mean. Beyond one standard deviation, for example, the shapes start to exhibit significant skewness and more complexity, reflecting increasingly irregular rupture processes. These irregular types comprise a non-negligible proportion of the entire earthquake population (e.g. 32% if counting those outside radius 1), which should be interpreted by more sophisticated rupture models.

The STF model derived by the VAE approach aims to quantify the first and second order features of global earthquakes' STFs, which is similar to the STF model by Meier et al (2017). However, the two models differ in some important aspects. For example, in addition to the median STF, Meier et al (2017) quantified the statistical fluctuations, which is found to be multiplicative and Gaussian-like. Their model considers a real STF as the median STF perturbed by random fluctuations at all frequencies. In comparison, our model produces smoother STFs and the high-frequency roughness of real STFs is assimilated in the misfit and viewed as part of earthquake complexity (Figures 1-3). Moreover, our model has two controlling parameters to reconstruct the STFs and take a misfit metric to measure the excursion, whereas the model of Meier et al. (2017) has controlling parameters as many as the fluctuation phases at all frequencies. These differences are essentially sourced from different decomposition schemes of real STFs resulted from the respective methods.

*Implications for earthquake early warning*

The diversity of temporal moment release patterns imposes a limit on magnitude determinism, i.e. the predictability of earthquake size before the rupture is complete. A near isosceles triangular shape averaged from all STFs suggests that approximately half the duration is required to predict final magnitude (Meier et al., 2017). In addition, many symmetric events observed in the model exhibit a low-amplitude onset acceleration, which may also lead to magnitude underestimate in early warning. For the runaway events, the early amplitude is particularly small and long and the peak moment rate arrives much later. This runaway behavior could be caused by dynamic weakening mechanisms during the rupture development , such as flash heating and thermal pressurization, resulting in the break of strong asperities in the later rupture stage (Denolle et al., 2015). Alternatively, it could be also caused by triggering a later large asperity by an early small asperity. In this case, both ruptures are so close in time that the moment release appears to be one peak. More generally, triggering among asperities with different sizes and spatial separations can result in other types of events as well. Recent discoveries of similar initial waveforms between large and small earthquakes imply that whether or not a small event can develop into a big one could be in part a stochastic result (Okuda and Ide, 2018; Ide, 2019). Hence, this type of events poses a greater challenge for early warning.

Although STFs predicted by the Brune and Haskell models (Haskell, 1964; Brune, 1970) as well as those empirically derived tend to emphasize the importance of symmetric and long-tail STFs (Tanioka and Ruff, 1997), our results show that the population of the runaway type is actually comparable to that of the symmetric type. The examples of large runaway events include the 1996 Mw 7.7 and 2001 Mw 7.6 Peru, 2010 Mw 8.8 Chile, and 2011 Mw 7.3 Honshu earthquakes (Figure S4). In addition to the runaway type, complex events represented in $Q_1$ have subevents with unknown relative size and timing, which can further confuse early warning systems. It seems that there is no effective way to diagnose the event type when the rupture is developing, making early magnitude estimation more challenging. Recent studies also show that that the absolute duration can vary significantly even for earthquakes with similar magnitudes (Vallée, 2013; Sallarès and Ranero, 2019), which further decreases magnitude predictability beyond the discussed STF shape diversity. Therefore, early estimates of earthquake magnitude would expectedly often excurse, even though it could be partly inferred (Melgar and Hayes, 2019).

*Potentials for revealing earthquake mechanics*

An important question in earthquake science is whether or not rupture processes are magnitude-dependent (Meier et al., 2017; Ye et al., 2018; Melgar and Hayes, 2019; Renou et al., 2019). Figure 2a shows stark contrast in the numbers of M>8 events in $Z_1>0$ and $Z_1<0$ quadrants, implying a plausible preferential rupture mode for M>8 events. In fact, we observe that the largest earthquakes seem to shift systematically to the negative $Z_1$ direction (Figure 4). We estimate the statistical significance of this trend by bootstrap tests. To reduce the impact of scarcity of large-magnitude events, in each test, 100 events are randomly drawn in each magnitude bin (Figure 4a and b) for calculation of Spearman correlation and p value. For bins with less than 100 events, all the events in the bins are used. This procedure is repeated 1,000 times. The results show that $Z_1$ has correlation $0.20 \pm 0.03$ with magnitude and p value $10^{-8\pm2}$, suggesting a statistically significant pattern shift along the $Z_1$ direction (Figure 4). In contrast, $Z_2$ has correlation $0.067 \pm 0.03$ with magnitude and p value $10^{-1.3\pm0.8}$, suggesting negligible change along the $Z_2$ direction. This magnitude-dependent $Z_1$ distribution implies that the largest earthquakes seemingly prefer to begin with small events (symmetric or run-away types) rather than release most of the energy in the early stage (long-tail type). An admissible explanation is that a relatively high level of rupture momentum and dynamic weakening is likely needed to activate and break unusually large and/or strong asperities.

More generally, the encoder-decoder system provides an effective tool to investigate potential pattern variations with source parameters and thus could offer useful insights into the physics of rupture processes. It also provides a convenient tool to evaluate the generality and peculiarity of particular events in the context of historical observations in a uniform framework. Our study illustrates that generative unsupervised machine learning could be powerful in uncovering underlying collective patterns of high-dimensional seismic data.

**Acknowledgements**

I would like to thank the editor Germán Prieto, Jean-Paul Ampuero and an anonymous reviewer for their constructive comments. This work has benefited from discussion with Jiuxun Yin, Hiroo Kanamori, Men-Andrin Meier, Han Yue, and Lingling Ye. I thank Martin Vallee and Lingling Ye for providing their source time function databases and thank Xin Cui for help in the bootstrapping tests. This work is by supported by the research startup fund from USTC (Grant No. KY2080000079).

**Data Availability**

The SCARDEC database is available at http://scardec.projects.sismo.ipgp.fr/ (last accessed on September 3, 2021). The STFs of megathrust earthquakes can be accessed from the supplementary material in Ye et al. (2016) (doi.org/10.1002/2015JB012426, last accessed on September 3, 2021).

**Author contributions**

Z. L. conceive the idea, analyze the data and write the manuscript.

**Competing interests**

The author declares no competing interests.

## References


Ammon, C. J. (2005). Rupture Process of the 2004 Sumatra-Andaman Earthquake, *Science* **308**, no. 5725, 1133–1139, doi: 10.1126/science.1112260.

Ammon, C. J., H. Kanamori, and T. Lay (2008). A great earthquake doublet and seismic stress transfer cycle in the central Kuril islands, *Nature* **451**, no. 7178, 561–565, doi: 10.1038/nature06521.

Ammon, C. J., H. Kanamori, T. Lay, and A. A. Velasco (2006). The 17 July 2006 Java tsunami earthquake, *Geophys. Res. Lett.* **33**, no. 24, doi: 10.1029/2006GL028005.

Brune, J. N. (1970). Tectonic stress and the spectra of seismic shear waves from earthquakes, *J. Geophys. Res. 1896-1977* **75**, no. 26, 4997–5009, doi: 10.1029/JB075i026p04997.

Cheng, X., and K. Jiang (2020). Crustal model in eastern Qinghai-Tibet plateau and western Yangtze craton based on conditional variational autoencoder, *Phys. Earth Planet. Inter.* **309**, 106584, doi: 10.1016/j.pepi.2020.106584.

Denolle, M. A. (2019). Energetic Onset of Earthquakes, *Geophys. Res. Lett.* **46**, no. 5, 2458–2466, doi: 10.1029/2018GL080687.

Denolle, M. A., W. Fan, and P. M. Shearer (2015). Dynamics of the 2015 M7.8 Nepal earthquake, *Geophys. Res. Lett.* **42**, no. 18, 7467–7475, doi: 10.1002/2015GL065336.

Dokht Dolatabadi Esfahani, R., K. Vogel, F. Cotton, M. Ohrnberger, F. Scherbaum, and M. Kriegerowski (2021). Exploring the Dimensionality of Ground-Motion Data by Applying Autoencoder Techniques, *Bull. Seismol. Soc. Am.*, doi: 10.1785/0120200285.

Duputel, Z., V. C. Tsai, L. Rivera, and H. Kanamori (2013). Using centroid time-delays to characterize source durations and identify earthquakes with unique characteristics, *Earth Planet. Sci. Lett.* **374**, 92–100, doi: 10.1016/j.epsl.2013.05.024.

Furlong, K. P., T. Lay, and C. J. Ammon (2009). A Great Earthquake Rupture Across a Rapidly Evolving Three-Plate Boundary, *Science* **324**, no. 5924, 226–229, doi: 10.1126/science.1167476.

Haskell, N. A. (1964). Total energy and energy spectral density of elastic wave radiation from propagating faults, *Bull. Seismol. Soc. Am.* **54**, no. 6A, 1811–1841.

Houston, H. (2001). Influence of depth, focal mechanism, and tectonic setting on the shape and duration of earthquake source time functions, *J. Geophys. Res. Solid Earth* **106**, no. B6, 11137–11150, doi: 10.1029/2000JB900468.

Houston, H., and J. E. Vidale (1994). The Temporal Distribution of Seismic Radiation During Deep Earthquake Rupture, *Science* **265**, no. 5173, 771–774, doi: 10.1126/science.265.5173.771.

Ide, S. (2019). Frequent observations of identical onsets of large and small earthquakes, 7772, *Nature* **573**, no. 7772, 112–116, doi: 10.1038/s41586-019-1508-5.

Kingma, D. P., and J. Ba (2017). Adam: A Method for Stochastic Optimization, *ArXiv14126980 Cs*.

Kingma, D. P., and M. Welling (2014). Auto-Encoding Variational Bayes, in *Proceedings of the International Conference on Learning Representations (ICLR)*.

Li, H., and S. Misra (2017). Prediction of Subsurface NMR T2 Distributions in a Shale Petroleum System Using Variational Autoencoder-Based Neural Networks, *IEEE Geosci. Remote Sens. Lett.* **14**, no. 12, 2395–2397, doi: 10.1109/LGRS.2017.2766130.

Liu, M., D. Grana, and L. P. de Figueiredo (2021). Uncertainty quantification in stochastic inversion with dimensionality reduction using variational autoencoder, *GEOPHYSICS*, 1–65, doi: 10.1190/geo2021-0138.1.

Lopez-Alvis, J., E. Laloy, F. Nguyen, and T. Hermans (2021). Deep generative models in inversion: The impact of the generator's nonlinearity and development of a new approach based on a variational autoencoder, *Comput. Geosci.* **152**, 104762, doi: 10.1016/j.cageo.2021.104762.

Meier, M.-A., J. P. Ampuero, and T. H. Heaton (2017). The hidden simplicity of subduction megathrust earthquakes, *Science* **357**, no. 6357, 1277–1281, doi: 10.1126/science.aan5643.

Melgar, D., and G. P. Hayes (2019). Characterizing large earthquakes before rupture is complete, *Sci. Adv.* **5**, no. 5, eaav2032, doi: 10.1126/sciadv.aav2032.

Meng, L., J.-P. Ampuero, J. Stock, Z. Duputel, Y. Luo, and V. C. Tsai (2012). Earthquake in a Maze: Compressional Rupture Branching During the 2012 Mw 8.6 Sumatra Earthquake, *Science* **337**, no. 6095, 724–726, doi: 10.1126/science.1224030.

Okuda, T., and S. Ide (2018). Hierarchical rupture growth evidenced by the initial seismic waveforms, 1, *Nat. Commun.* **9**, no. 1, 3714, doi: 10.1038/s41467-018-06168-3.

Persh, S. E., and H. Houston (2004). Deep earthquake rupture histories determined by global stacking of broadband P waveforms, *J. Geophys. Res. Solid Earth* **109**, no. B4, doi: https://doi.org/10.1029/2003JB002762.

Renou, J., M. Vallée, and P. Dublanchet (2019). How Does Seismic Rupture Accelerate? Observational Insights From Earthquake Source Time Functions, *J. Geophys. Res. Solid Earth* **124**, no. 8, 8942–8952, doi: 10.1029/2019JB018045.

Ross, Z. E., B. Idini, Z. Jia, O. L. Stephenson, M. Zhong, X. Wang, Z. Zhan, M. Simons, E. J. Fielding, S.-H. Yun, *et al.* (2019). Hierarchical interlocked orthogonal faulting in the 2019 Ridgecrest earthquake sequence, *Science* **366**, no. 6463, 346–351, doi: 10.1126/science.aaz0109.

Sallarès, V., and C. R. Ranero (2019). Upper-plate rigidity determines depth-varying rupture behaviour of megathrust earthquakes, *Nature* **576**, no. 7785, 96–101, doi: 10.1038/s41586-019-1784-0.

Shearer, P. M., G. A. Prieto, and E. Hauksson (2006). Comprehensive analysis of earthquake source spectra in southern California, *J. Geophys. Res. Solid Earth* **111**, no. B6, doi: 10.1029/2005JB003979.

Tanioka, Y., and L. J. Ruff (1997). Source Time Functions, *Seismol. Res. Lett.* **68**, no. 3, 386–400, doi: 10.1785/gssrl.68.3.386.

Vallée, M. (2013). Source time function properties indicate a strain drop independent of earthquake depth and magnitude, *Nat. Commun.* **4**, no. 1, 2606, doi: 10.1038/ncomms3606.

Vallée, M., and V. Douet (2016). A new database of source time functions (STFs) extracted from the SCARDEC method, *Phys. Earth Planet. Inter.* **257**, 149–157, doi: 10.1016/j.pepi.2016.05.012.

Ye, L., H. Kanamori, and T. Lay (2018). Global variations of large megathrust earthquake rupture characteristics, *Sci. Adv.* **4**, no. 3, eaao4915, doi: 10.1126/sciadv.aao4915.

Ye, L., T. Lay, H. Kanamori, and L. Rivera (2016). Rupture characteristics of major and great ( $M_w$ $\geq$ 7.0) megathrust earthquakes from 1990 to 2015: 1. Source parameter scaling relationships, *J. Geophys. Res. Solid Earth* **121**, no. 2, 826–844, doi: 10.1002/2015JB012426.

Yin, J., Z. Li, and M. A. Denolle (2021). Source Time Function Clustering Reveals Patterns in Earthquake Dynamics, *Seismol. Res. Lett.* **92**, no. 4, 2343–2353.

## Figures

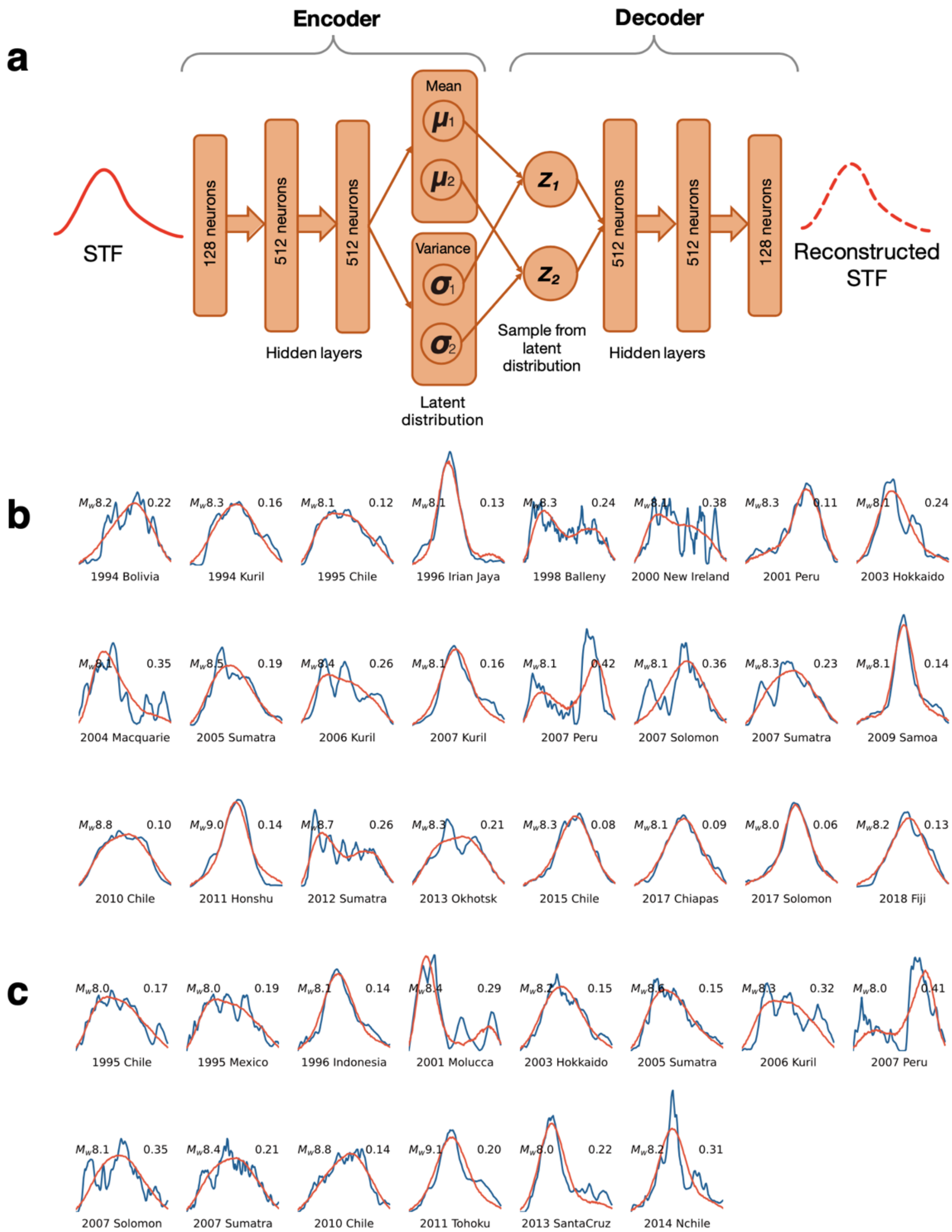


**Figure 1. Variational autoencoder (VAE) for earthquake source time functions (STFs).** a. VAE architecture. Both of the decoder and encoder consist of two fully connected layers with 512 neurons each. The bottleneck consists of two latent variables constrained to follow normal distribution. b. Original STFs (blue) and VAE reconstructed STFs (red) from SCARDEC. The numbers in the top right mark the misfits. c. Same as b but for the STF database of Ye et al. (2016) (referred to as YE2016 thereinafter).

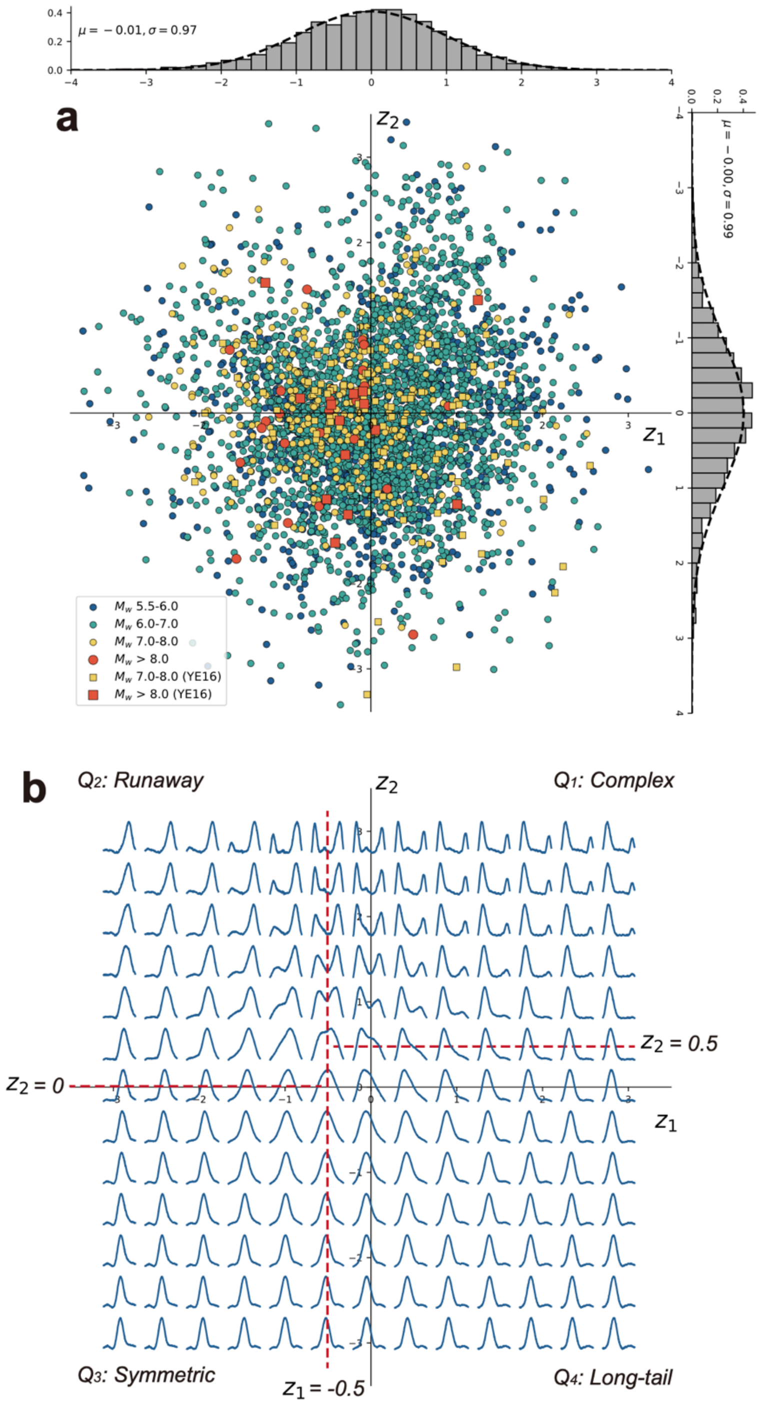


**Figure 2. The latent representation and the standard model of STFs.** a. Low-dimensional latent representations of SCARDEC (dots) and YE2016 (squares) STFs. The population density in both $Z_1$ and $Z_2$ follows normal distribution. b. The standard STF model reconstructed from virtual latent values. The model shows systematic variations of STFs: complex type in $Q_1$, runaway type in $Q_2$, symmetric type in $Q_3$, and long-tail type in $Q_4$.

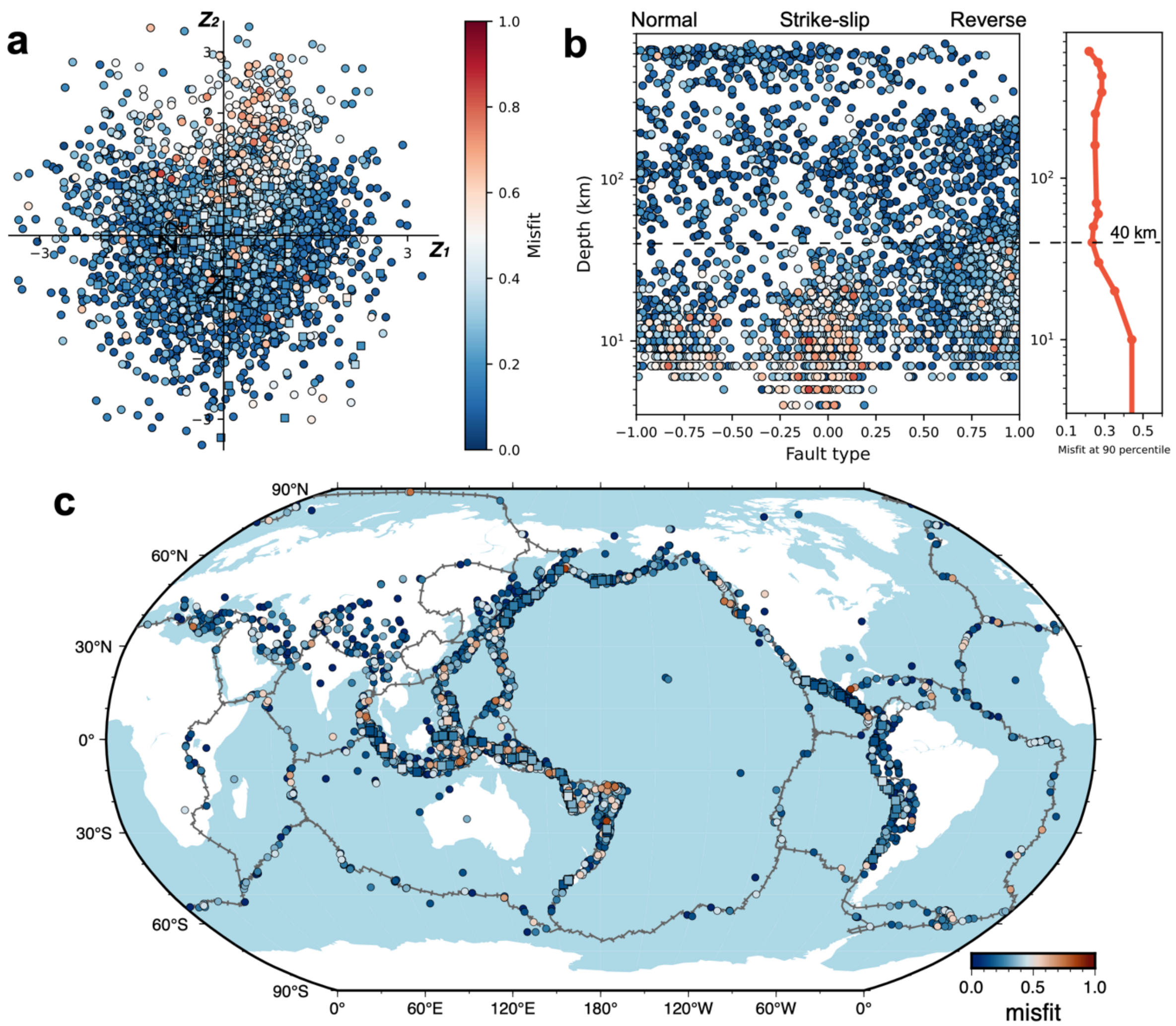


**Figure 3. Reconstruction misfit as a proxy of unusual earthquakes.** a. Reconstruction misfits of all the SCARDEC (dots) and YE2016 (squares) events in latent space. Note that most high-misfits are located in $Q_1$ and some are in other quadrants. b. Reconstruction misfit as a function of earthquake depth and focal mechanisms. The definition of fault type follows Shearer et al. (2006). On the right is the median misfit across depth. The depth at 40 km marks the change point of earthquake complexity. c. Geographic distribution of reconstruction misfit of global earthquakes. Note that the high-misfits are predominantly located in the northern boundaries of the Australian plate and Southeast Asia.

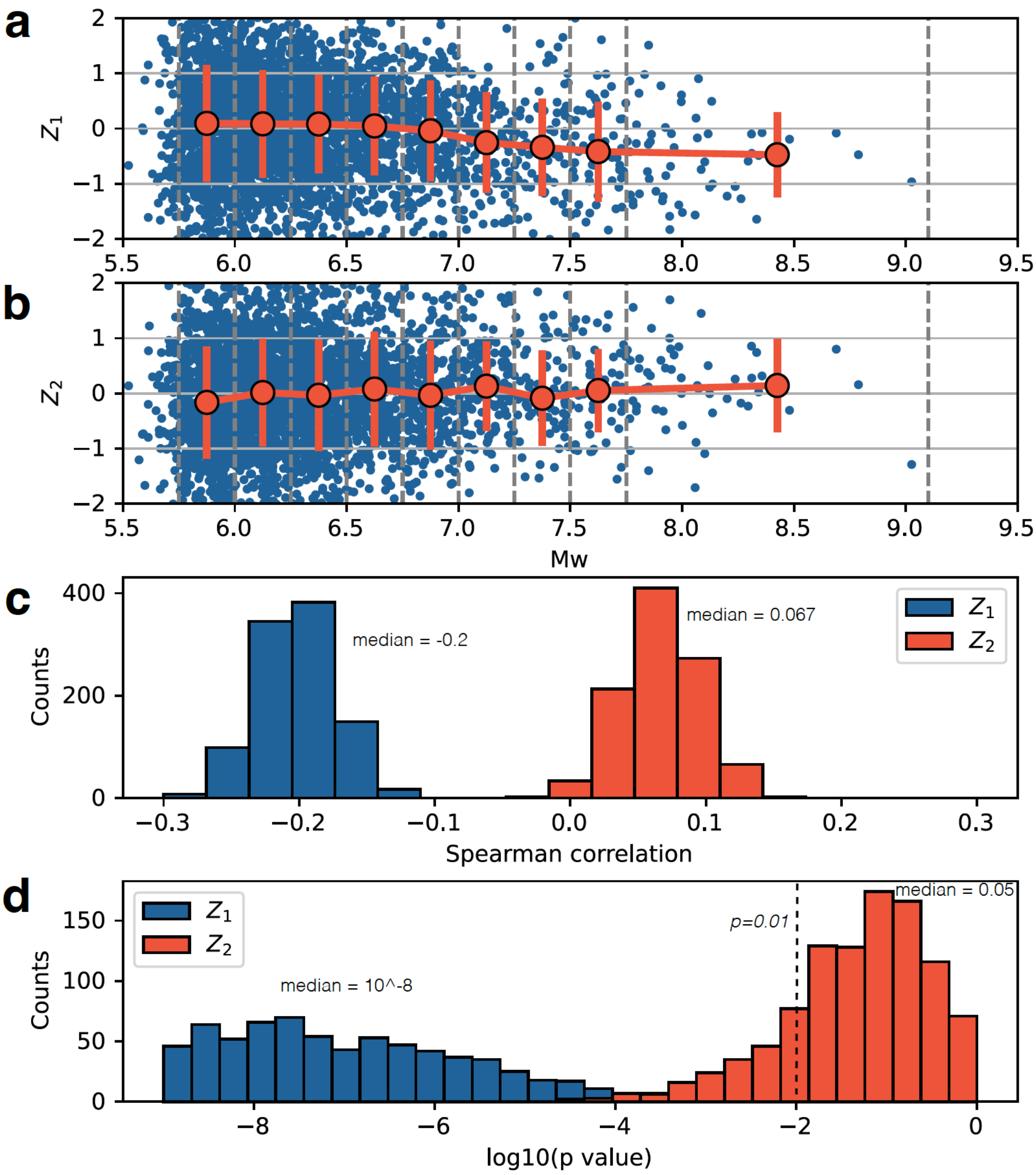


**Figure 4. Dependencies of latent variables $Z_1$ and $Z_2$ on magnitude.** a. Blue dots represent $Z_1$ of individual earthquakes. Red dots and bars represent the mean and standard deviation in each magnitude bin bracketed by dashed gray lines. b. Similar symbol representation as in a but for $Z_2$. c. Histograms of Spearman correlations between $Z_1$, $Z_2$ and magnitude from bootstrapping tests. d. Histograms of p values for hypothesis test in which null hypothesis is that $Z_1$, $Z_2$ are uncorrelated with magnitude. In each test, 100 events are randomly selected in each magnitude bin (for bins with less than 100 events, all within the bins are used) to calculate the correlation and p-value, which is repeated 1,000 times.